Experimental study of the phase transformation plasticity of 16MND5 low carbon steel induced by proportional and nonproportional biaxial loading paths

Michel Coret, Sylvain Calloch, Alain Combescure

Experimental study of the phase transformation plasticity of 16MND5 low carbon steel induced by proportional and nonproportional biaxial loading paths

M. Coret [a], S . C a l l o c h [b], A. Combescure [a]

[a] *LaMCoS, CNRS UMR 5514, INSA, bâtiment J.C.A. Coulomb, 20, avenue Albert Einstein, 69621 Villeurbanne cedex, France*

[b] *LMT-Cachan, ENS. Cachan/CNRS UMR 8535/université Paris 6, 61, avenue du Président Wilson, 94235 Cachan cedex, France*

This article deals with the multiphasic, anisothermal behavior of 16MND5 steel (used in French nuclear reactor vessels) under complex loading. We are focusing more specifically on transformation plasticity induced by proportional or nonproportional biaxial loading. The first part briefly reviews the experimental setup we have been using. The second part concerns the study of transformation-induced plasticity under constant stress in the cases of bainitic, martensitic and austenitic transformations. These tests enabled us to identify Leblond's transformation plasticity model. The final part presents tests on the transformation plasticity induced by nonproportional biaxial loading and their comparison with the previously identified model.

Keywords: A-phase transformation; A-thermomechanical processes; B-constitutive behavior; B-metallic materials; C-mechanical testing

1. Introduction

For a number of years, much research has been devoted to the thermomechanical behavior of materials during solid–solid phase changes. The main objective is to be able to predict the distortions and residual stresses in a structure following a welding or heat treatment process. This is a relatively ambitious prospect as at least three physical phenomena must be taken into account: the thermal loading, the mechanical loading and the phase transformation mechanisms (Inoue and Wang, 1985). Let us recall that the slightest stress applied during a phase transformation results in a residual deformation called "TRansformation-Induced Plasticity" (TRIP). Two physical interpretations of this phenomenon were given by Greenwood and Johnson (1965) for the case of diffusion transformation and by Magee (1966) for the case of martensitic transformation.

A number of experimental studies were conducted (Abrassart, 1972; Desalos, 1981; Hamata et al., 1991; Videau et al., 1996; Taleb et al., 2000; Denis et al., 1987b; Martinez, 1999), leading to numerous models (Greenwood and Johnson, 1965; Leblond et al., 1989a; Inoue and Wang, 1985; Hamata et al., 1991; Fischer et al., 2000b; Cherkaoui and Berveiller, 2000; Nagayama et al., 2000, 2002; Tanaka et al., 2003; Taleb and Sidoroff, 2003). However, while real-life cases necessarily involve non-constant multiaxial stress states due to nonhomogeneous temperature fields, virtually all these experiments were performed under constant uniaxial loading. Yet, the tension–torsion tests by Videau seem to indicate that the multiaxial character of the loading influences transformation-induced plasticity in the case of martensitic transformation. Therefore, it appears essential

Table 1
Chemical composition of 16MND5 in % mass (Mizushima, 1984)

C	S	P	Si	Mn	Ni	Cr	Mo	Cu	Co	Fe
0.17	0.002	0.004	0.25	1.44	0.75	0.20	0.51	0.01	0.004	balance

to provide new results on little-studied transformations, such as austenitic transformation, and to conduct tests under loading situations closer to reality.

This article consists of three parts. The first part concerns mostly the material, the experimental setup and the phase transformations being studied. The second part presents the results of numerous tests performed in order to characterize transformation plasticity under constant biaxial stress during bainitic, martensitic and austenitic transformations. These tests were used to identify Leblond's transformation plasticity model. The final part concerns the transformation plasticity induced by nonproportional loading during bainitic transformation. Results are presented for three types of loading and compared to the response of the model.

2. The experimental setup

2.1. Material and test specimen

The material being studied is 16MND5 steel used in French PWR vessels. This is a low-alloy, low-carbon steel whose chemical composition is given in Table 1. The tension–torsion test specimen is a thin tube connected to two massive heads by a wide fillet, which ensures that the state of stress in the central zone is homogeneous (Coret et al., 2002). We will assume throughout that the shear stress is constant across the thickness.

$$\sigma = \begin{bmatrix} 0 & 0 & 0 \\ 0 & 0 & \tau \\ 0 & \tau & \sigma \end{bmatrix}_{(\vec{e}_r, \vec{e}_\theta, \vec{e}_z)}$$

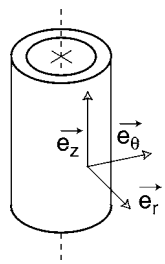

Height: 35 mm
Diameters:
$\phi_{\text{int}} = 23.4$ mm
$\phi_{\text{ext}} = 25.4$ mm

2.2. Mechanical and thermal loads

The mechanical loading was applied using an electro-hydraulic tension–torsion servo testing machine with a maximum capacity of 100 kN in tension/compression and 1.2 kN m in torsion. Heating was provided by induction, which required the development of a specific inductor (Coret et al., 2002) to insure a homogeneous temperature field in the measurement zone. Thus, the test sample could be heated to temperatures greater than the austenitic transformation temperature ($T > 800\,^\circ\text{C}$). Finally, for the fastest cooling stages ($< -5\,^\circ\text{C}\,\text{s}^{-1}$), the injection of gaseous argon at the center of the test sample (Fig. 1) enabled cooling rates of the order of $-50\,^\circ\text{C}\,\text{s}^{-1}$.

2.3. Measurements

During each test, the following parameters were monitored continuously: the tension force F (giving the normal stress σ), the torque C (giving the tangent stress τ), the axial and shear strains ε, γ and the temperatures T in 12 points.

3. The transformations being considered

In the rest of the paper, we will study transformation-induced plasticity through three transformations which are likely to occur for the steel grade we are interested in: one transformation during the heating stage and two transformations during cooling. Table 2 summarizes the characteristics of these transformations.

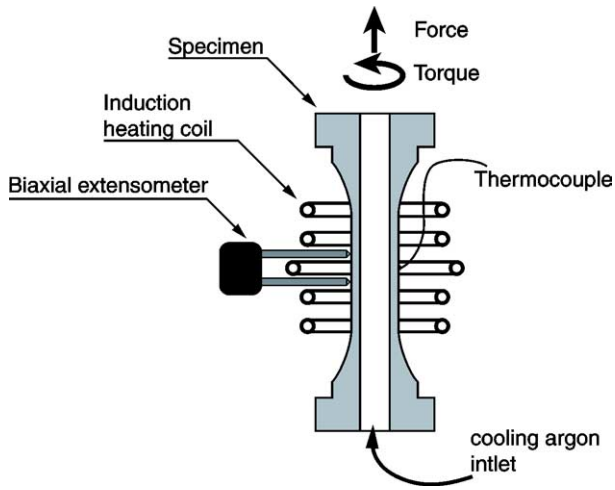

Fig. 1. The experimental device.

Table 2
Summary of the characteristics

	$\dot{T}_{\text{mean}}$ ($^\circ$C s^{-1})	Value
Ac_1	10	680 °C
Ac_3	10	800 °C
Bs	−3	550 °C
Ms	−48	400 °C
α_α	–	16.1×10^{-6} °C^{-1}
α_γ	–	22.6×10^{-6} °C^{-1}

3.1. Austenitic transformation

Austenite is a solid solution of carbon in γ iron which remains stable at high temperatures. During this transformation, which occurs upon heating, α iron (body-centered cubic structure), which was stable at low temperatures, turns into γ iron (face-centered cubic structure). At the rates we are considering, of the order of 10 °C s^{-1}, the phase change begins at 680 °C and ends around 800 °C, as shown in Figs. 2(b) and 2(a).

3.2. Martensitic transformation

During very rapid cooling, carbon does not have time to diffuse and, therefore, causes carbon–supersaturated ferrite to appear below temperature *Ms*. In the case of ferritic steels such as 16MND5, this transformation is possible only for very high cooling rates. Our tests were performed at average rates of about 50 °C s^{-1}. Fig. 2(a) shows one of these tests. As often, a very small residual strain remains at the end of the dilatometry test.

3.3. Bainitic transformation

At lower cooling rates, small carbon–supersaturated ferrite platelets appear at temperatures higher than *Ms*, but these can last only if their carbon can be expelled: this is the bainitic transformation mechanism. The transformation does not progress through seeding and growth, but through the multiplication of thin ferrite platelets. In our case, this transformation takes place at rates of the order of 3 °C s^{-1}. Fig. 2(b) shows a free dilatometry obtained for a bainitic transformation.

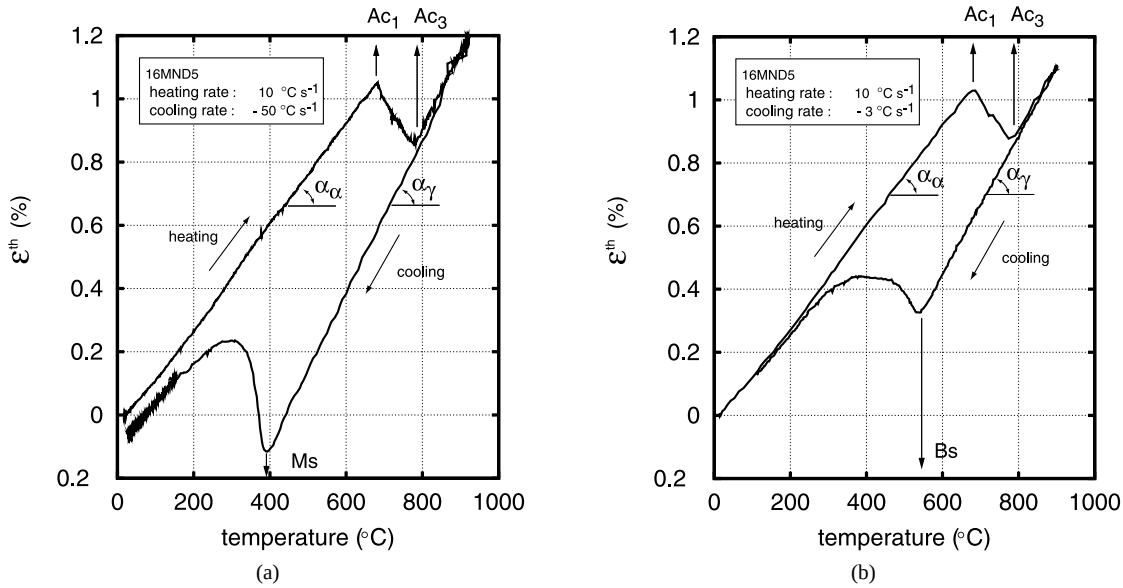

Fig. 2. Free dilatometries. (a) Martensitic transformation; (b) Bainitic transformation.

Table 3
Mechanical loading sequence applied in the stress plane $(\sigma, \tau\sqrt{3})$

Cycle	σ	τ
1	0	0
2	σ	0
3	0	τ
4	$\sigma/\sqrt{2}$	$\tau/\sqrt{2}$
5	$-\sigma$	0
6	$-\sigma/\sqrt{2}$	$\tau/\sqrt{2}$

such that $\tau\sqrt{3} = \sigma$

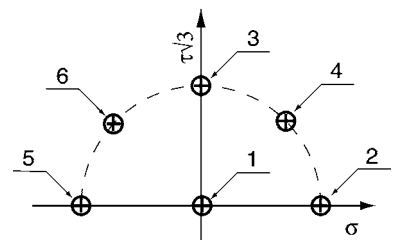

Fig. 3. Loading sequence.

4. Dilatometry under constant stress

4.1. Loading paths

The first tests we conducted were intended to characterize transformation-induced plasticity under constant (uniaxial or biaxial) stress states. Therefore, these tests can be compared with existing uniaxial test results (Martinez, 1999; Cavallo, 1998; Grostabussiat-Petit, 2000). Moreover, they enable us to check whether transformation-induced plasticity is indeed, as predicted by Leblond's model (Leblond et al., 1989a), proportional to the deviator of the macroscopic stresses.

For each transformation, the same loading sequence was applied to the test sample. A sequence was composed of six stages during which the same thermal loading was applied. Furthermore, all tests were conducted for the same equivalent stress in the Von Mises' sense. During each cycle, a different mechanical solicitation was applied, as shown in Table 3.

The first stage was a free dilatometry during which all deformations are, therefore, due to thermal effects. Stages 2 and 5 were unidirectional tension and compression tests. Stage 3 was a shear test. Finally, Stages 4 and 6 corresponded to truly biaxial tension or compression loading combined with shear (Fig. 3). Stresses were applied just prior to the phase transformation at a rate of about 100 MPa s^{-1}. For the bainitic and martensitic transformations, the stresses were brought down to zero at the end of the tests (around 100 °C). However, in the case of austenitic transformation, the stresses were relieved at the end of the transformation to prevent high temperature creeping phenomena from occurring.

The stress levels applied in each sequence are listed in Table 4. As an indication, let us recall that the conventional 0.2% yield strength of austenite is (Grostabussiat-Petit, 2000; Martinez, 1999; Waeckel, 1994): $\sigma_\gamma^y = 100$ MPa at 600 °C, 150 MPa at 400 °C and 60 MPa at 800 °C.

Table 4
The tests performed

Transformation	σ_{eq} (MPa)
Bainitic	30, 45, 60
Martensitic	40, 50, 60, 70, 80
Austenitic	10, 15, 20, 30

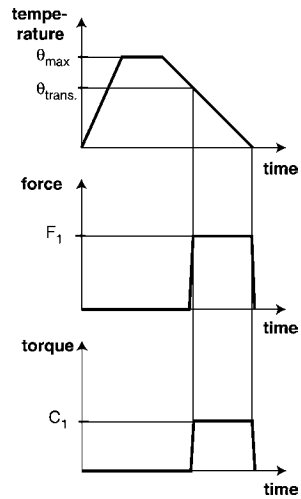

Fig. 4. Description of the loading applied at each stage.

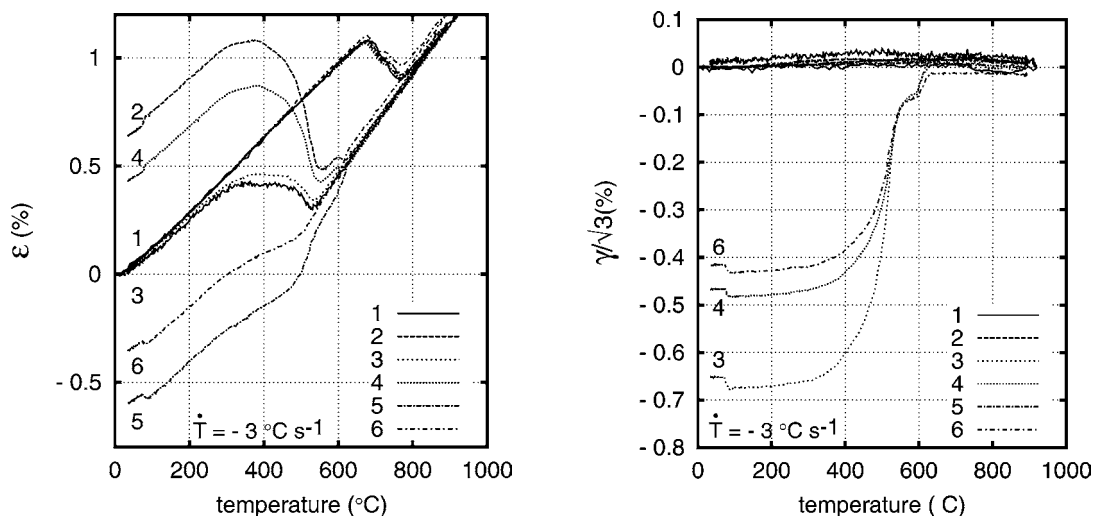

(a) (b)

Fig. 5. Evolution of the total strain vs. the temperature for each loading stage ($\sigma_{eq} = 60$ MPa). (a) Axial strain; (b) Shear strain.

4.2. Results from the tests – bainitic transformation

On Fig. 5, we represented the axial and shear strains measured during the test at $\sigma_{eq} = 60$ MPa against the temperature. One can see that for $\sigma = 0$ (Stages 1 and 3) the axial strain is equal to zero. Similarly, when no shear stress is applied (Stages 1, 2 and 5), the shear strain is zero. Finally, when combined tension and shear loads are applied (Stages 4 and 6), axial and shear strains develop. Let us also note that the kinetics of the transformation is slightly affected, by the applied stress.

4.2.1. Extraction of transformation-induced plasticity

We suppose in that part that the strains are small. Our objective is to extract from the total strain the transformation-induced plastic strain.

Let us recall that in Leblond's model (Leblond et al., 1989a) the strains are partitioned, through time integration, as follows:

$$\mathbb{\varepsilon}^{\mathrm{t}} = \mathbb{\varepsilon}^{\mathrm{e}} + \mathbb{\varepsilon}^{\mathrm{thm}} + \mathbb{\varepsilon}^{\mathrm{cp}}_{T} + \mathbb{\varepsilon}^{\mathrm{cp}}_{\sigma} + \mathbb{\varepsilon}^{\mathrm{tp}}. \tag{1}$$

(1) $\mathbb{\varepsilon}^{\mathrm{t}}$ is the total strain.
(2) $\mathbb{\varepsilon}^{\mathrm{thm}}$ is the thermal and metallurgical strain, deduced from the free dilatometry (Cycle 1).
(3) $\mathbb{\varepsilon}^{\mathrm{e}}$ is the elastic strain, calculated using the elastic properties of each phase.
We will assume that the elastic properties are the same in each phase and depend only on the temperature. The Young's modulus depends on the temperature and is calculated using the expression (Martinez, 1999):

$$E(T) = 2.08 \times 10^5 - 1.90 \times 10^2 T + 1.19 T^2 - 2.82 \times 10^{-3} T^3 + 1.66 \times 10^{-6} T^4,$$

where E is in MPa and T in °C. We will also assume that the Poisson's ratio ν is constant and equal to 0.3.
(4) $\mathbb{\varepsilon}^{\mathrm{cp}}_{\sigma}$ and $\mathbb{\varepsilon}^{\mathrm{cp}}_{T}$ are classical plasticity terms.
In the case for our experiments we have $\|\dot{\mathbb{\varepsilon}}^{\mathrm{cp}}_{\sigma} + \dot{\mathbb{\varepsilon}}^{\mathrm{cp}}_{T}\| < 0.1\|\dot{\mathbb{\varepsilon}}^{\mathrm{tp}}\|$ (Coret, 2001).
(5) $\mathbb{\varepsilon}^{\mathrm{tp}}$ is the transformation plasticity strain, whose rate is proportional to $\dot{z}_\gamma$. $\dot{z}_\gamma$ is defined as the austenite volume fraction rate.

Finally, the transformation-induced plastic strains can be determined through:

$$\begin{aligned} \varepsilon^{\mathrm{tp}}(T) &= \varepsilon(T) - \varepsilon^{\mathrm{e}}(T) - \varepsilon^{\mathrm{thm}}(T), \\ \gamma^{\mathrm{tp}}(T) &= \gamma(T) - \gamma^{\mathrm{e}}(T). \end{aligned} \tag{2}$$

Fig. 6 shows the axial and shear plastic strains calculated from Eq. (2) against the temperature.

Let us compare the experimental results with the predictions from Leblond's model. First, we will look at the final values of the residual strain from transformation-induced plasticity; then, we will compare the evolution of the measured strains with those predicted by the model.

In the case of small applied stresses and for $z_\gamma > 0.03$ one has (Leblond et al., 1989a):

$$\dot{\mathbb{\varepsilon}}^{\mathrm{tp}} = 3\frac{\Delta\varepsilon^{T}_{\alpha,\gamma}}{\sigma^{y}_{\gamma}} \ln(z_\gamma)\dot{z}_\gamma \mathbb{S},$$

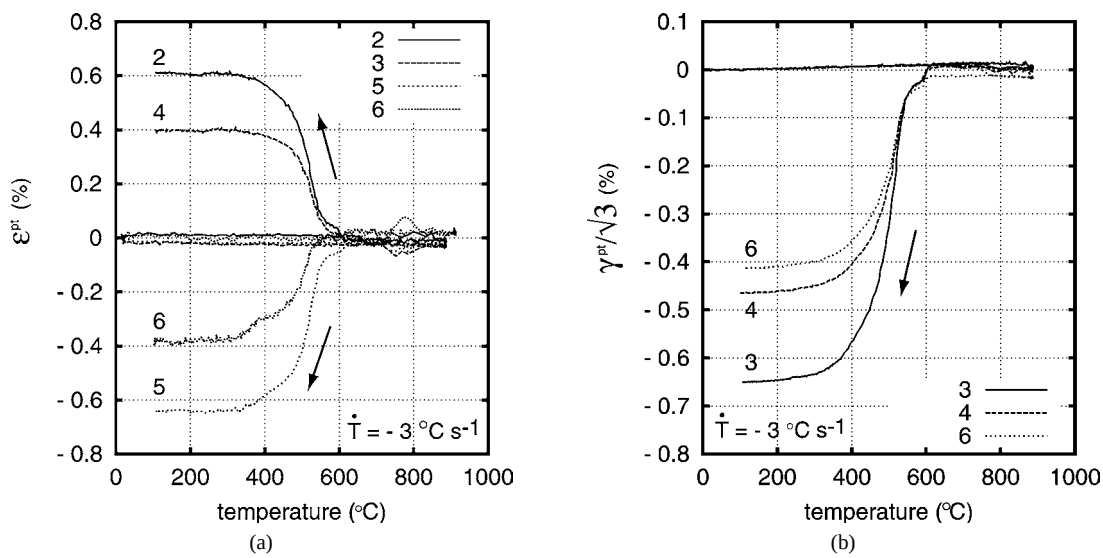

Fig. 6. Transformation-induced plastic strains vs. the temperature ($\sigma_{\mathrm{eq}} = 60$ MPa). (a) Axial strain; (b) Shear strain.

where $\Delta\varepsilon^T_{\alpha,\gamma}$ is the difference of thermal strain between the 2 phases at the temperature T.

$$\int_{t_0}^{t_1} \dot{\boldsymbol{\varepsilon}}^{\mathrm{tp}}\,\mathrm{d}t = \int_{t_0}^{t_1} 3\frac{\Delta\varepsilon^T_{\alpha,\gamma}}{\sigma^y_\gamma}\ln(z_\gamma)\dot{z}_\gamma\,\mathbb{S}\,\mathrm{d}t = 3\mathbb{S}\Delta\varepsilon^T_{\alpha,\gamma}\int_{t_0}^{t_1}\frac{1}{\sigma^y_\gamma}\ln(z_\gamma)\dot{z}_\gamma\,\mathrm{d}t \tag{3}$$

if we consider $\Delta\varepsilon^T_{\alpha,\gamma}$ constant during the transformation

$$\boldsymbol{\varepsilon}^{\mathrm{tp}} = 3\mathbb{S}\Delta\varepsilon^T_{\alpha,\gamma}\int_{t_0}^{t_1}\frac{1}{\sigma^y_\gamma}\ln(z_\gamma)\dot{z}_\gamma\,\mathrm{d}t. \tag{4}$$

For all the tests performed at a given cooling rate, the transformation is the same; therefore, the following integral is a constant:

$$I = \int_{t_0}^{t_1}\frac{1}{\sigma^y_\gamma}\ln(z_\gamma)\dot{z}_\gamma\,\mathrm{d}t = \text{Constant}.$$

Finally, if we write:

$$I' = 3\Delta\varepsilon^T_{\alpha,\gamma} I$$

we get:

$$\varepsilon^{\mathrm{tp}}_{\mathrm{eq}} = \frac{2}{3}I'\sigma_{\mathrm{eq}} \tag{5}$$

with $\varepsilon^{\mathrm{tp}}_{\mathrm{eq}} = \sqrt{\varepsilon^{\mathrm{tp}2} + \gamma^{\mathrm{tp}2}/3}$ and $\sigma_{\mathrm{eq}} = \sqrt{\sigma^2 + 3\tau^2}$.

This equation shows that for any equivalent stress in Von Mises' sense, the associated transformation-induced plastic strain is the same regardless of the stress state. Furthermore, in the case of small loads, the strain is proportional to the applied stress.

Fig. 7 shows the final equivalent transformation-induced plastic strain against the applied stress. One can see on this graph that for any test at a given equivalent stress the equivalent strains are practically the same. Furthermore, the transformation-induced plastic strain is proportional to the level of the equivalent stress in Von Mises' sense.

4.2.2. Identification of Leblond's model

We are going to present the application of basic perfect plasticity Leblond's model to interpret the experimental results. This approach is rather coarse but needs only the yields stress of the austenite. We know the variation of compactness of the phases for our material (see Section 3.3) and, since we are considering a complete transformation, z_γ varies between 0 and 1. Therefore, we are missing only the yield strength of austenite. A first method consists of seeking this value in the literature. Many authors, e.g. Martinez (1999), Cavallo (1998), Desalos (1981) or Leblond et al. (1989a), proposed values of the yield strength of austenite between 110 MPa and 145 MPa for temperatures of the order of 500 °C. Let us note that this yield strength

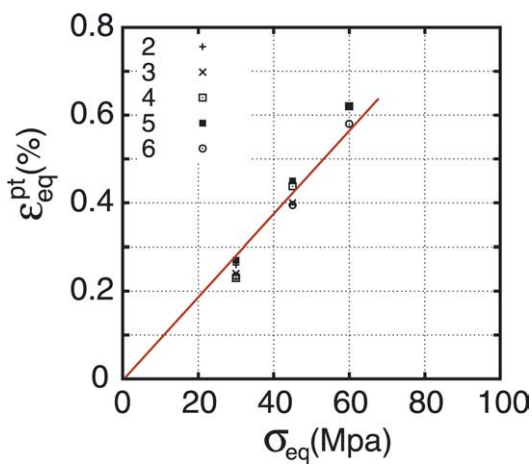

Fig. 7. Equivalent (in Von Mises' sense) transformation-induced plastic strain vs. equivalent (in Von Mises' sense) stress.

Table 5
Equivalent transformation-induced plasticity (calculated and from tests) vs. the equivalent stress

σ_{eq} (MPa)	Calculated ε_{eq}^{tp} (%)	Experimental ε_{eq}^{tp} (%)
30	0.3	0.25
45	0.45	0.42
60	0.6	0.6

is particularly difficult to evaluate as austenite is unstable at low temperatures and, therefore, characterization tests are very delicate, if not impossible. One approach consists of cooling the austenite down to the desired temperature, then stopping the cooling and performing a characterization test (one can refer to, e.g., Petit's thesis (Grostabussiat-Petit, 2000)). The problem with such a characterization is that it is performed at high strain rate. Is the result still valid at a lower rate? This can be problematic if the material is viscous. Moreover, direct characterization of a phase is impossible when a phase change is taking place. In such a case, it is useful to solve an inverse problem to retrieve the characteristics of a phase.

In view of these problems, we propose simply to fit Leblond's model to our tests by determining the yield strength of austenite, which we assume to remain constant during the transformation. In the case where σ_γ^y is constant, we get:

$$\varepsilon_{eq}^{tp} = 2\frac{\Delta\varepsilon_{\alpha,\gamma}^T}{\sigma_\gamma^y}\left[\int_{t_0}^{t_1} \ln(z_\gamma)\dot{z}_\gamma \,\mathrm{d}t\right]\sigma_{eq}$$

i.e.:

$$\varepsilon_{eq}^{tp} = 2\frac{\Delta\varepsilon_{\alpha,\gamma}^T}{\sigma_\gamma^y}\left[\int_{0}^{1} \ln(z_\gamma)\,\mathrm{d}z_\gamma\right]\sigma_{eq}.$$

Therefore, by integration:

$$\varepsilon_{eq}^{tp}(z_\gamma) - \varepsilon_{eq}^{tp}(0) = 2\frac{\Delta\varepsilon_{\alpha,\gamma}^T}{\sigma_\gamma^y}\left[z\big(\ln(z)-1\big)\right]_0^{z_\gamma}\sigma_{eq} \tag{6}$$

and

$$\varepsilon_{eq}^{tp}(1) - \varepsilon_{eq}^{tp}(0) = -2\frac{\Delta\varepsilon_{\alpha,\gamma}^T}{\sigma_\gamma^y}\sigma_{eq}. \tag{7}$$

Thus, we obtain:

$$\boxed{\sigma_\gamma^y = 140 \text{ MPa}}$$

for temperatures ranging from 300 to 600 °C, which is close to the highest value what can be found in the literature. Then, the comparison with experimental results can be made (Table 5).

One can also plot the evolution of transformation-induced plasticity against the temperature and the applied loading and compare this evolution with the experimental results (Fig. 8). One can see in this figure that the measured and calculated strains are relatively close. The final values are good because these are the experimental results on which the model was identified. Moreover, one can note that the evolution of strains is properly represented by Leblond's model. However, the simulation appears to work better for axial strains than for shear strains.

4.3. Results from the tests – martensitic transformation

This second part on constant stress tests concerns the martensitic transformation. The loading stages involved were exactly the same as those for the bainitic transformation. These tests were more difficult though because the transformation was very quick (cooling lasted 15 seconds and the transformation itself 2 to 3 seconds). An example of a test is shown in Fig. 9, in which the six loading cycles can be seen again. One can see that at the end of cooling, even in the free dilatometry stage, the strains do not return exactly to zero. In these tests, one can also observe that a tension or compression stress yields a pure axial strain. Similarly, a shear stress alone yields a pure shear strain. Moreover, the phase transformation seems unaffected by the applied stresses because the temperature at the onset of the transformation is the same for all the stages.

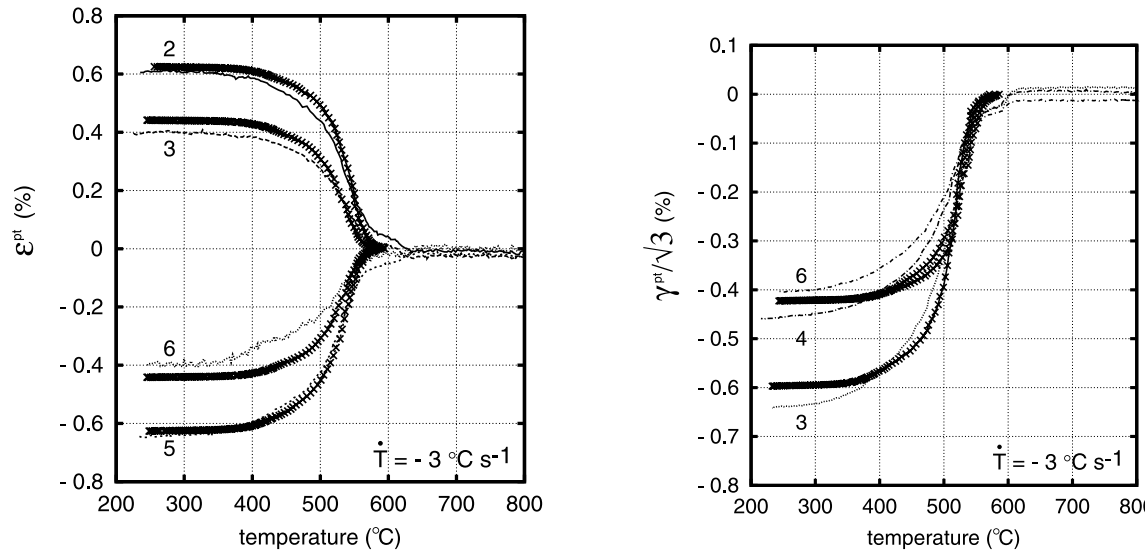

(a) (b)

Fig. 8. Transformation-induced plastic strains: comparison between experimental results and simulation ($\sigma_{eq} = 60$ MPa). (a) Axial strains; (b) Shear strains.

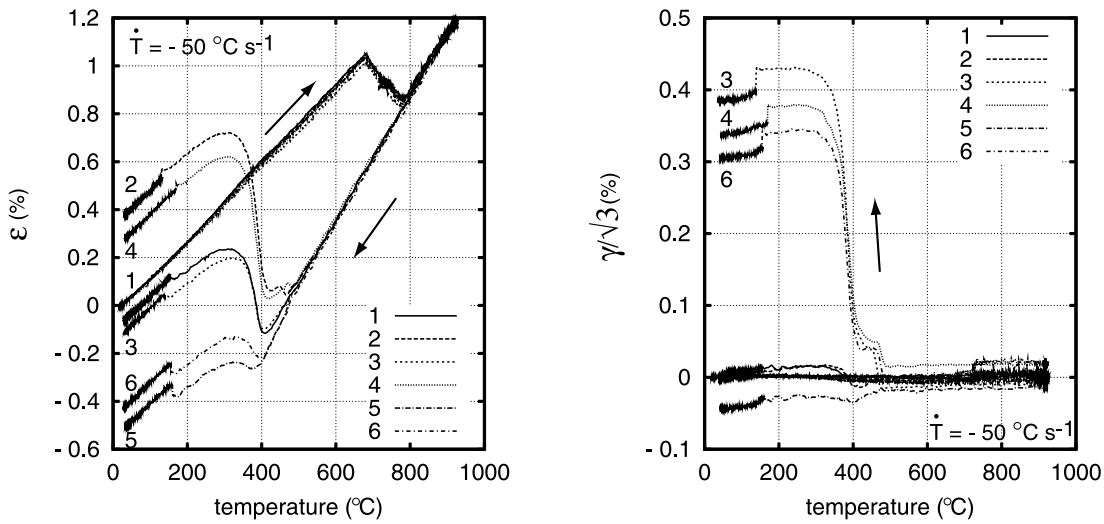

(a) (b)

Fig. 9. Evolutions of the total strains against the temperature and the loading ($\sigma_{eq} = 70$ MPa).

The same procedure as before was applied in order to extract the transformation-induced plastic strains from the total strains. The identification is done for applied stresses less than 70 MPa. For these tests, the strains thus obtained are represented in Fig. 10. One can also plot the equivalent transformation-induced plastic strain against the equivalent stress (Fig. 11). Up to 70 MPa, for the same applied equivalent stress, the strains are quite similar. Moreover, one can consider that the strains are proportional to the stresses and obtain:

$$\boxed{\sigma_\gamma^y = 210 \text{ MPa}}$$

Regarding the 80 MPa equivalent stress, one can make two remarks. First, the equivalent plastic strain seems to depend on the solicitation applied. This observation could corroborate those already made by Videau et al. (1996). We cannot be definite on this point for lack of sufficient results. More tests at stress levels equal to or greater than 80 MPa would give useful indications.

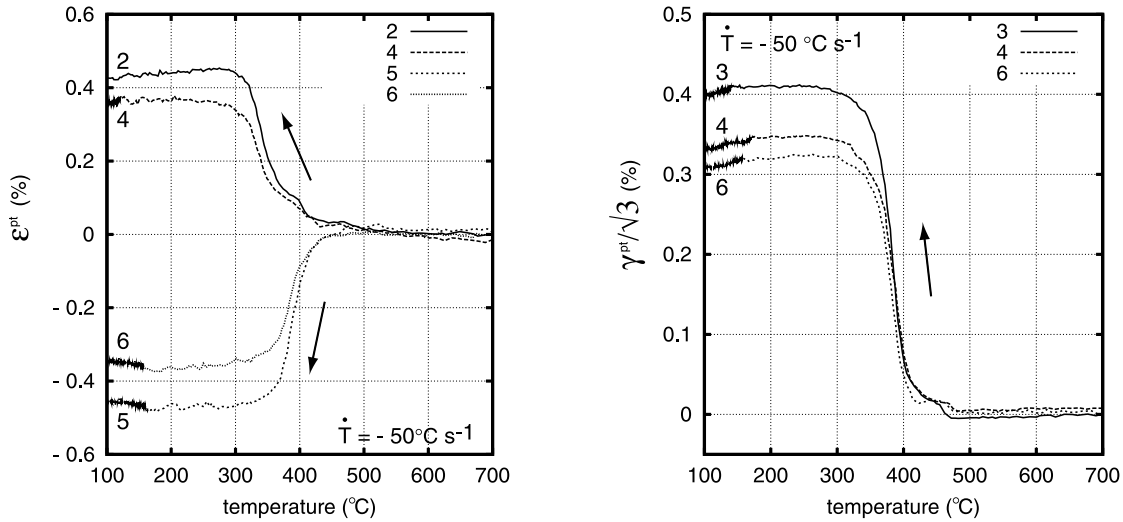

Fig. 10. Transformation-induced plastic strains ($\sigma_{\text{eq}} = 70$ MPa).

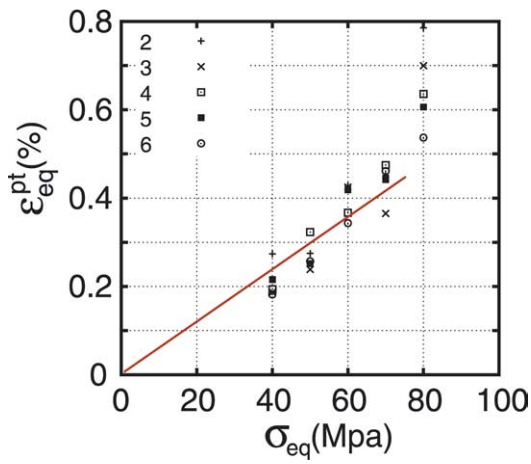

Fig. 11. Equivalent transformation-induced plastic strain vs. the equivalent stress.

Secondly, the mean value of the plastic strain seems to be greater than what would be predicted by a linear model. This confirms the observations by Leblond (1989a) and Taleb (2000).

4.4. Results from the tests – austenitic transformation

The final tests on transformation plasticity induced by constant biaxial stresses concern the austenitic transformation. As was the case for cooling transformations, one can speak of transformation-induced plasticity through heating, even though this case has been far less studied. Nevertheless, it appears important to take these phenomena into account when one wants to study thermomechanical rupture during or occurring beyond the transformation temperatures, for instance in severe accident over heating situation in a nuclear reactor. Here, the plasticity mechanisms involved can be only of the Greenwood and Johnson type since the new phase is formed through seeding and growth. Let us recall that, from a metallurgical point of view, such a transformation is very different from bainitic and martensitic transformations.

The tests performed during heating were very similar to those made during cooling. The load was applied just prior to the austenitic transformation (about 700 °C) and relieved immediately at the end of the transformation (about 800 °C). In this case, it was particularly important to end heating in a stress-free state in order not to induce viscoplastic flow of the austenite. Finally,

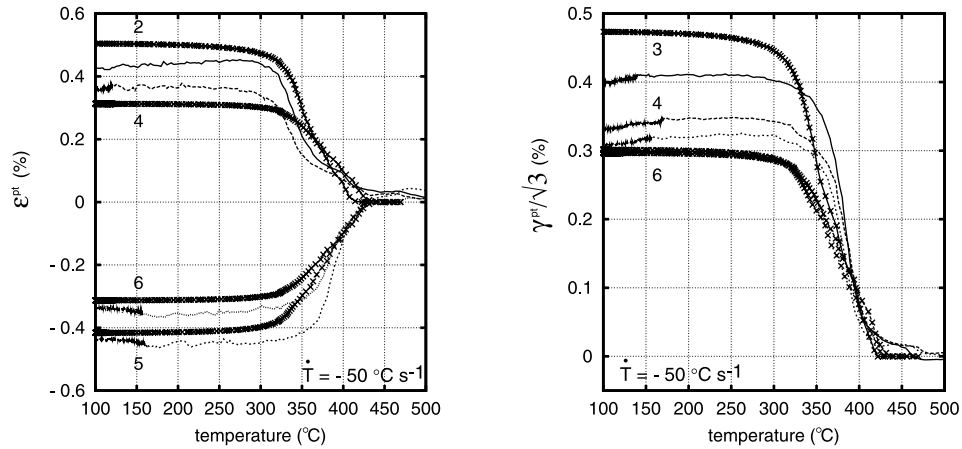

(a) (b)

Fig. 12. Transformation-induced plastic strains: comparison between experimental results and simulation ($\sigma_{eq} = 70$ MPa). (a) Axial strain; (b) Shear strain.

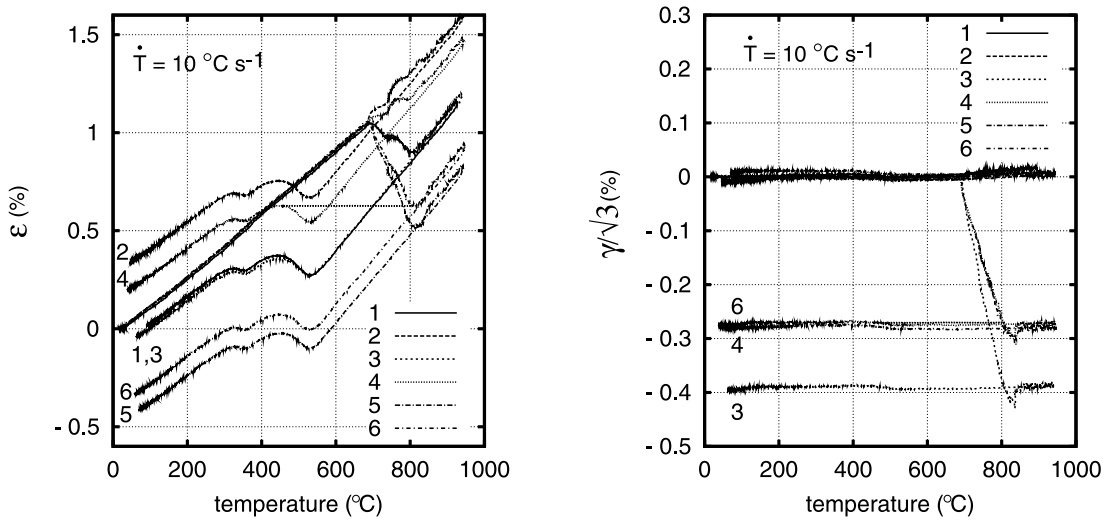

(a) (b)

Fig. 13. Evolutions of the total strains vs. the temperature and the loading ($\sigma_{eq} = 20$ MPa).

let us simply mention that, in these tests, the cooling rate was not controlled: heating was simply discontinued and the test sample cooled down by conduction and natural convection.

An example of a test is shown in Fig. 13. As for the cooling transformations, one can observe that an axial stress yields an axial plastic strain alone and a shear stress, a shear plastic strain alone. During cooling, all the curves are identical except for a translation. One can extract from these results, exactly as we did for the other transformations, the transformation-induced plastic strain term, which yields the curves shown in Fig. 14.

Leblond's model cannot be applied for the austenitic transformation, so, we do not try to identify this model in that case. We just plot the results on the graph $(\sigma_{eq}, \varepsilon_{eq}^{tp})$ given in Fig. 15. One observes that for a given equivalent stress all the points are near one another. Moreover, for the stress levels tested, the plastic strains are proportional to the stresses.

5. Bainitic transformation under nonproportional loading

Until now, as had been done in many other studies (Cavallo, 1998; Denis, 1996; Denis et al., 1985, 1987a; Desalos, 1981; Giusti, 1981; Greenwood and Johnson, 1965; Grostabussiat-Petit, 2000; Hamata et al., 1991; Magee, 1966; Martinez,

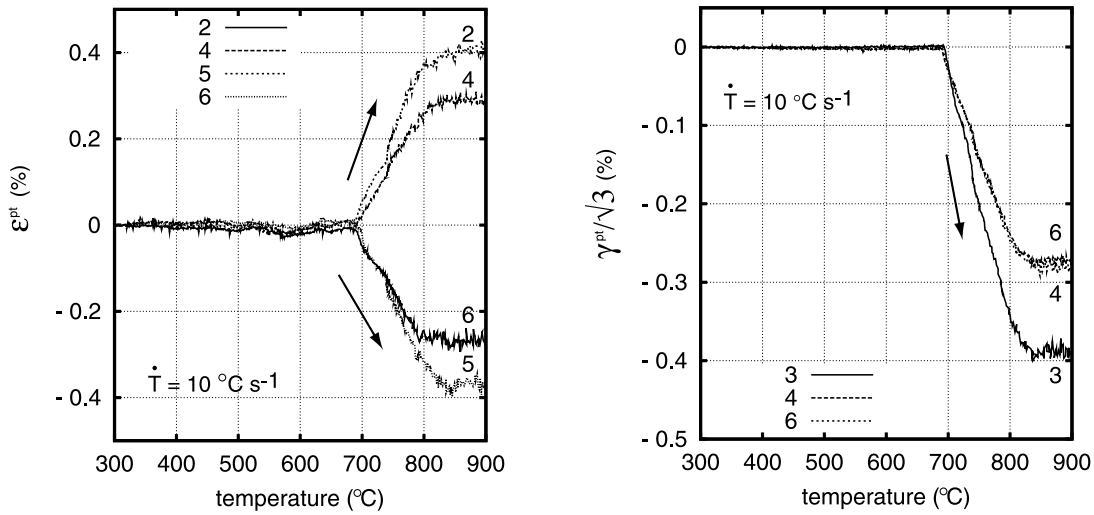

Fig. 14. Transformation-induced plastic strains ($\sigma_{eq} = 20$ MPa).

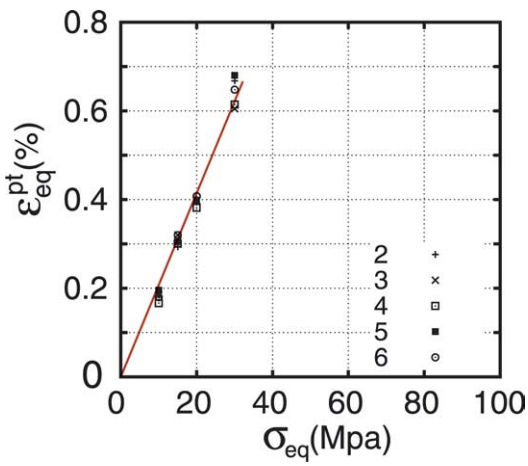

Fig. 15. Equivalent transformation-induced plastic strain vs. the equivalent stress.

1999; Taleb et al., 2000), we have been considering phase transformations under constant uniaxial stresses, as well as under constant biaxial stresses as in the works by Videau et al. (1996) and Coret et al. (2002). However, it is clear that during welding or heat treatment operations structures are subjected to nonhomogeneous temperature fields (Denis et al., 1987b; Fernandes et al., 1985; Habraken and Bourdouxhe, 1992; Inoue and Wang, 1985; Inoue et al., 1985; Martinez, 1999; Sjöström, 1985; Todinov, 1998). These solicitations generate complex stress fields which vary during the transformation. Therefore, it is necessary to acquire new experimental results which would be closer to actual situations. Accordingly, we tried to achieve loading cases in which the stresses would not be proportional to one another. Moreover, during these tests, at least one of the stress components would change sign. Thus, the loading possibilities become endless. We chose to concentrate our efforts on a single transformation, using several types of loading. This final test campaign was devoted to the transformation plasticity induced by complex load cases applied during the bainitic transformation. Some nonproportional tests on martensitic transformation are available in the these different works (Nagayama et al., 2000, 2001, 2002; Tanaka et al., 2003).

The loading paths. We used three types of loading whose paths were chosen in order to have:

(1) one component of the loading constant during the transformation;
(2) or piecewise constant components during the transformation;
(3) or both components varying during the transformation.

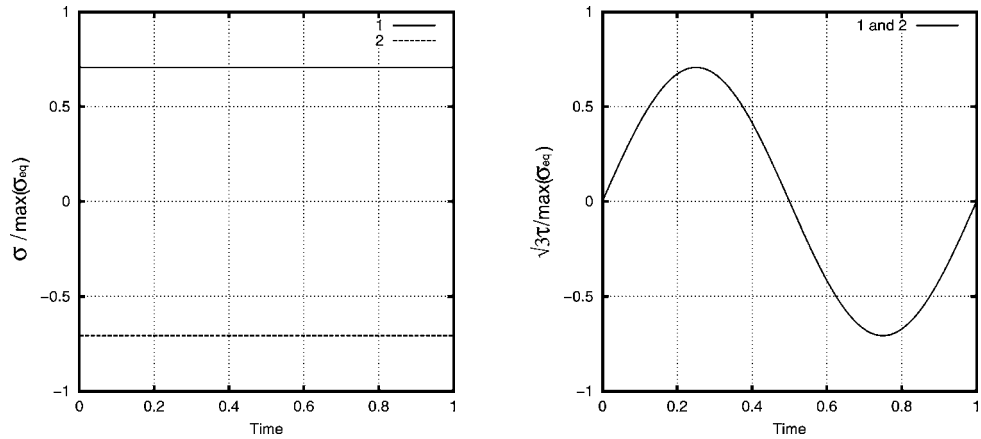

(a) (b)

Fig. 16. Type-1 and Type-2 *sine-constant* paths.

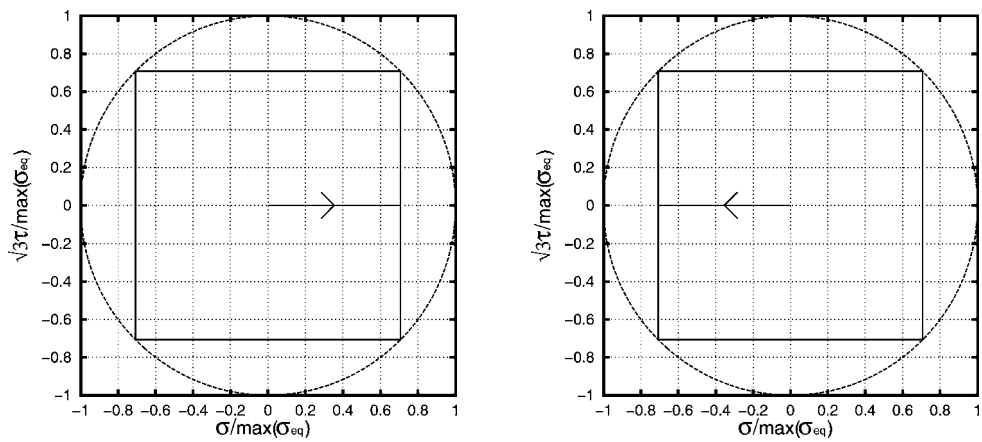

(a) (b)

Fig. 17. Type-1 and Type-2 *square* paths. (a) Square 1; (b) Square 2.

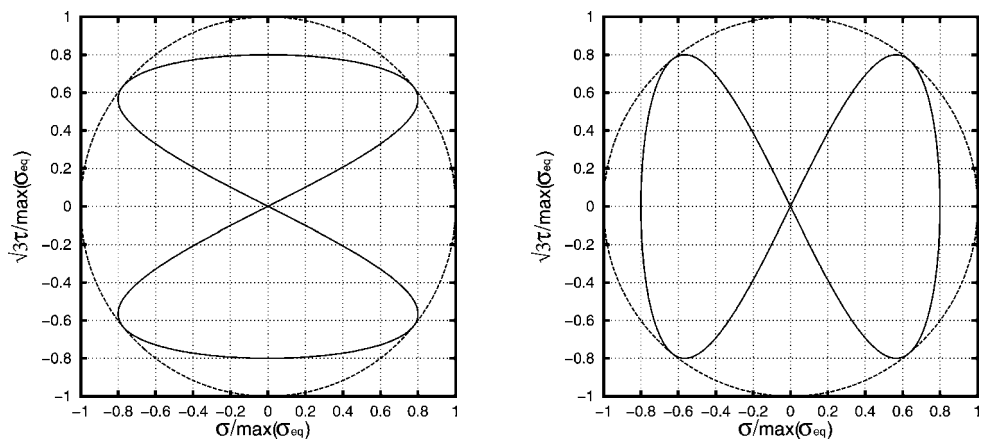

(a) (b)

Fig. 18. Type-1 and Type-2 *butterfly* paths. (a) Butterfly 1; (b) Butterfly 2.

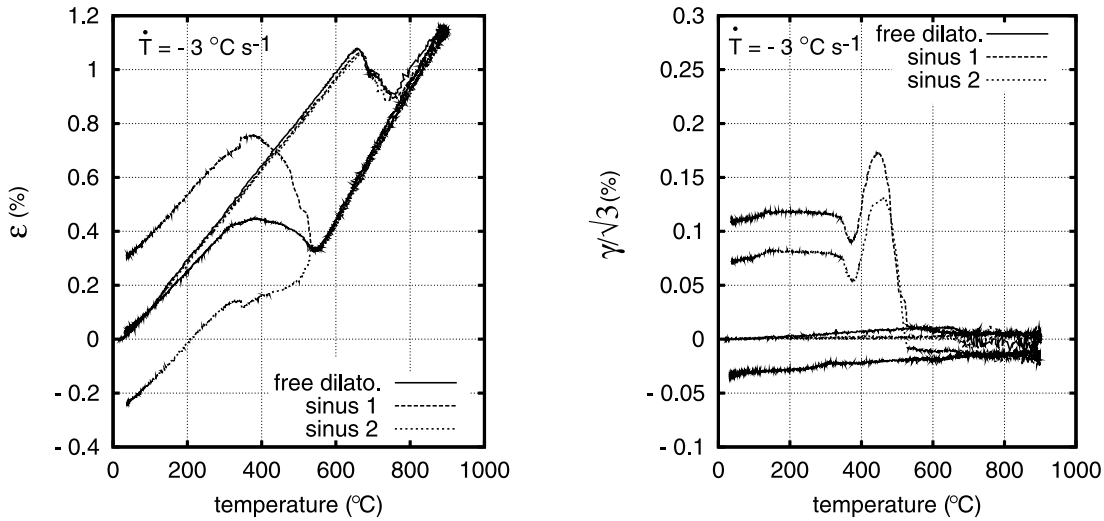

Fig. 19. Evolutions of the total strains vs. the temperature and the loading (*sine-constant* paths 1 and 2).

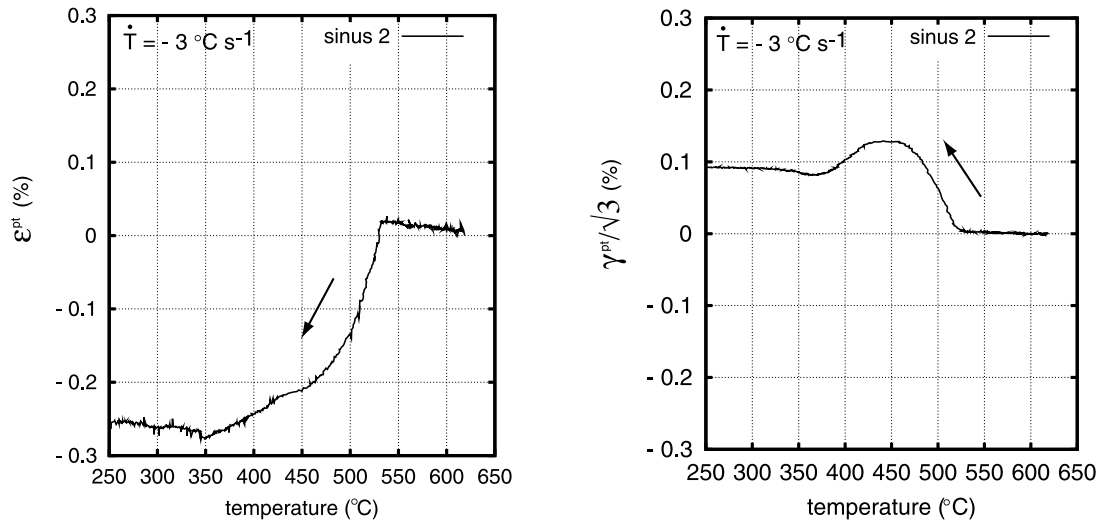

Fig. 20. Transformation-induced plastic strains vs. the temperature (*sine-constant* path 2).

The loading application starts at the beginning of the transformation ($\approx 550\,^{\circ}$C) and stops at the end ($\approx 400\,^{\circ}$C).

Finally, let us note that all the loading cases were preceded by a free dilatometry cycle, which was necessary in order to process the results.

The first load cases applied followed paths denoted *sine-constant* (Fig. 17). In these tests, one of the components was kept constant while the other varied sinusoidally. The subsequent load cases were *square* paths in the plane of the stresses ($\sigma, \tau\sqrt{3}$). Four types of *square* paths were applied (Fig. 17). These different load paths enabled us not to bias tension against compression. The last nonproportional tests were performed under *butterfly* load paths. Two types of tests were performed in which the butterflies take off either along the axis of the axial stresses or along the axis of the shear stresses (Fig. 18). In these tests, none of the stress components remained constant during the phase transformation.

5.1. Total strains and transformation-induced plastic strains

We present the results of one test sequence for each load type. First, we show the total axial and shear strains; then, the transformation-induced plasticity strains are extracted from the preceding curves.

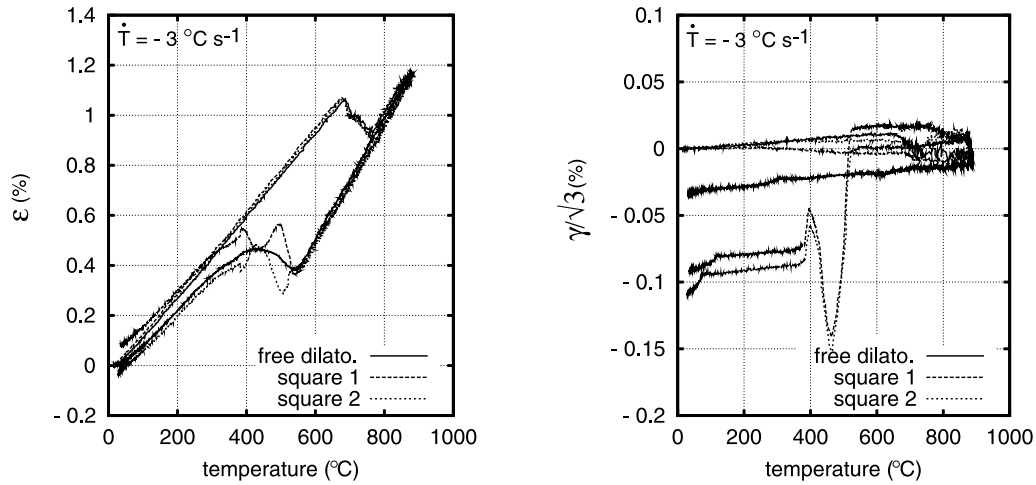

Fig. 21. Evolutions of the total strains vs. the temperature and the loading (*square* paths 1 and 2).

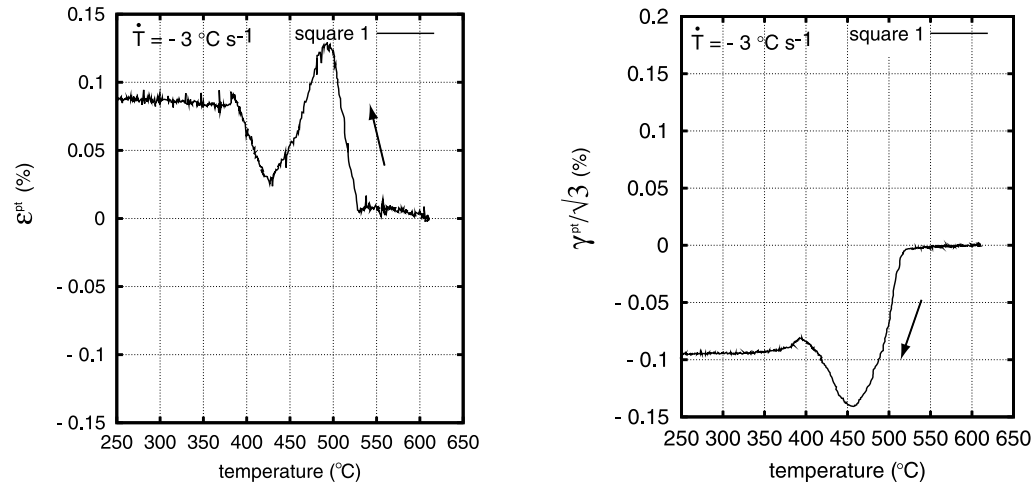

Fig. 22. Transformation-induced plastic strains vs. the temperature.

Sine-constant *load paths.* Figs. 19 and 20 show an example of a total strain measured during *sine-constant* loading paths 1 and 2. The axial strains fully resemble what we saw earlier, whereas the evolution of the shear strains is more complex. One can also observe on the latter that the evolutions for path 1 and path 2 are identical, which indicates the good repetitiveness of our tests. Then, we extracted the transformation-induced plastic strains from the total strains, which, in the case of path 2, led to Fig. 20. One can note that the transformation-induced strains are zero while there is no applied stress and that, beyond that, their evolution follows that of the stresses.

Square *load paths.* An example of a test result under *square* loading is given in Figs. 21 and 22. In this test, the maximum equivalent stress reached was 60 MPa and the stress evolved at a rate of 3 MPa s^{-1}. As before, one can observe that the evolution of the shear strain was identical for *square* paths 1 and 2, for which the evolution of the shear stress was identical.

Butterfly *load paths.* For this last loading type, we present an example of dilatometry results obtained for *butterfly* path 1 (Fig. 23). In this test, the maximum equivalent stress reached was 80 MPa and its evolution rate was 5 MPa s^{-1}. In this particular example, two butterfly cycles were applied during the transformation. Fig. 24 and show the evolution of the transformation-induced plastic strains extracted from the preceding curves.

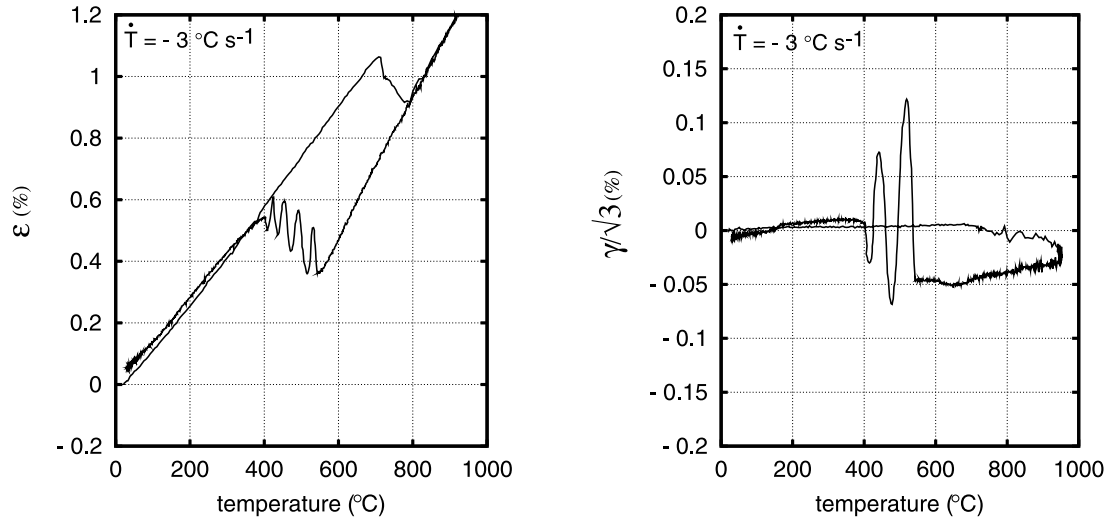

Fig. 23. Evolutions of the total strains vs. the temperature and the loading (*butterfly* path 1).

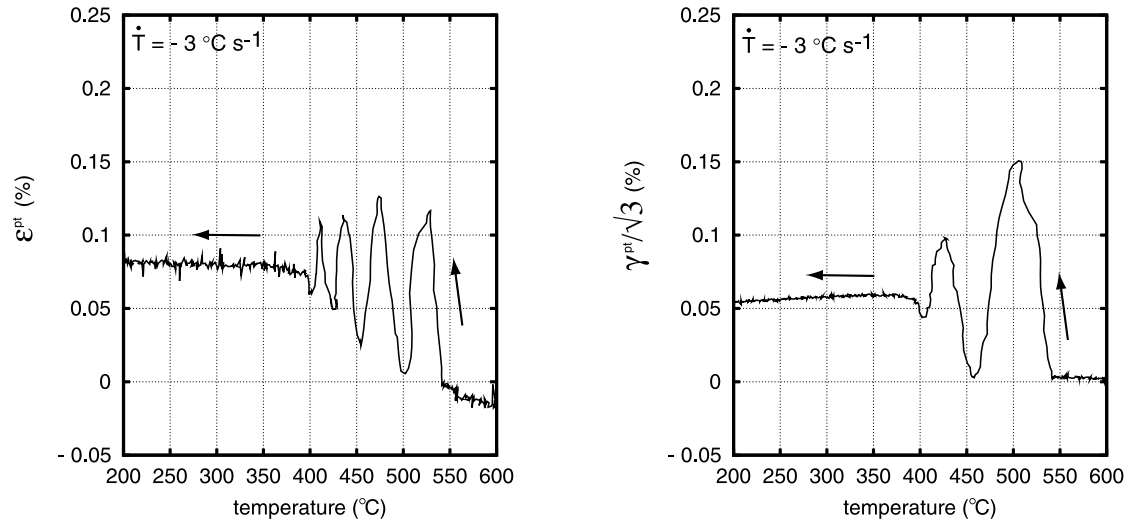

Fig. 24. Transformation-induced plastic strains (*butterfly* path 1).

5.1.1. Discussion of the nonproportional tests

In this section, we aim to compare the previous results obtained under nonproportional loading paths to the response of the first generation of TrIP model (without any backstress and Magee effect). We have chosen here to use Leblond's model (Leblond et al., 1989a) with the parameters identified with uniaxial transformation plasticity tests (see Section 4.2). For each loading case, the first figure gives the measured and calculated transformation-induced plasticity strains vs. the temperature. The second figure shows the shear plastic strains vs. the measured and calculated axial plastic strains. The comments on these figures can be found at the end of this chapter.

Sine-constant *loading paths.*
Figs. 25 and 26.

Square *loading paths.*
Figs. 27 and 28.

Butterfly *loading paths.* Figs. 29 and 30.

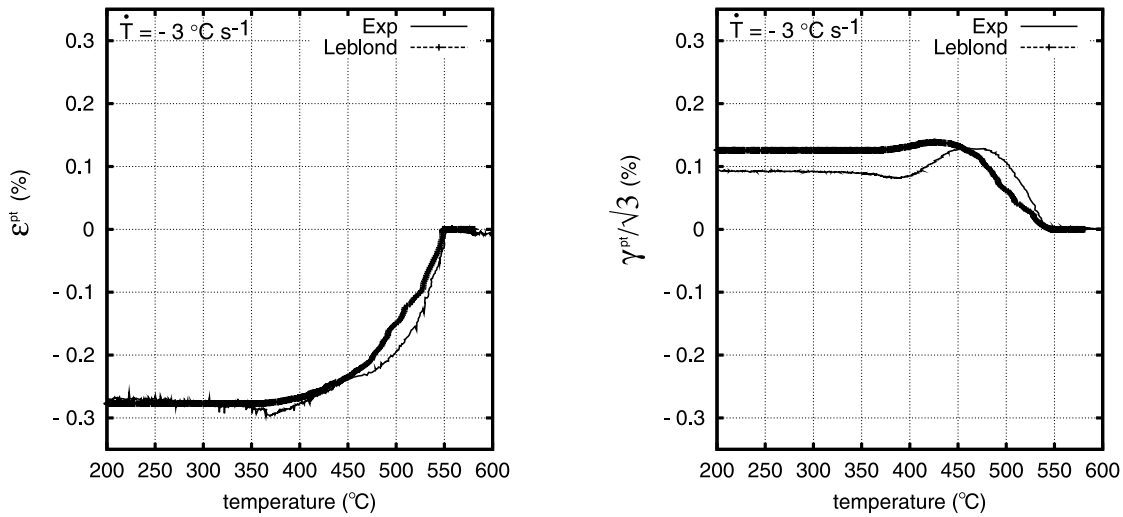

Fig. 25. Transformation-induced plastic strains – comparison with the prediction of Leblond's model (sine-constant paths 2).

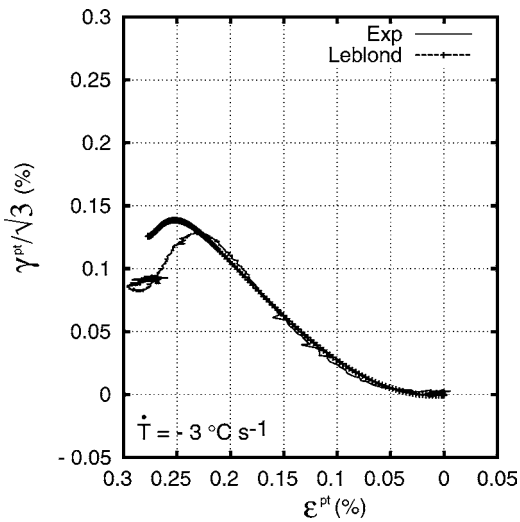

Fig. 26. Evolution of the shear component of the transformation-induced plastic strains vs. the axial component – comparison with the prediction of Leblond's model (sinus-constant paths 2).

Overall, the differences observed between the experimental results and the response of "ideal-plastic" Leblond's model are small, even though the identification was performed based on constant stress tests. Nevertheless, there are a few comments to be made. The *sine-constant* tests show that on the component for which the applied stress remains constant during the transformation the response of Leblond's model matches the experimental results perfectly. Conversely, slight discrepancies between the measured and calculated plastic strains occur when the derivative of the applied stresses changes sign (e.g. Figs. 27 and 28). Finally, in the *butterfly* loading case, in which the stresses vary sinusoidally, Leblond's model presents a "damping" effect which can be seen in Figs. 29 and 30. The response of the model predicts a rapid decay of the evolution of the plastic strains which we did not completely observe experimentally. These experimental results can be used as good base for identification and validation of the recently developed TrIP models (Fischer et al., 2000a, 2000b).

6. Conclusion

The objective of this article was twofold. First, we intended to produce new experimental results on transformation plasticity induced during martensitic, bainitic and austenitic transformations by constant biaxial stresses, but also by nonproportional

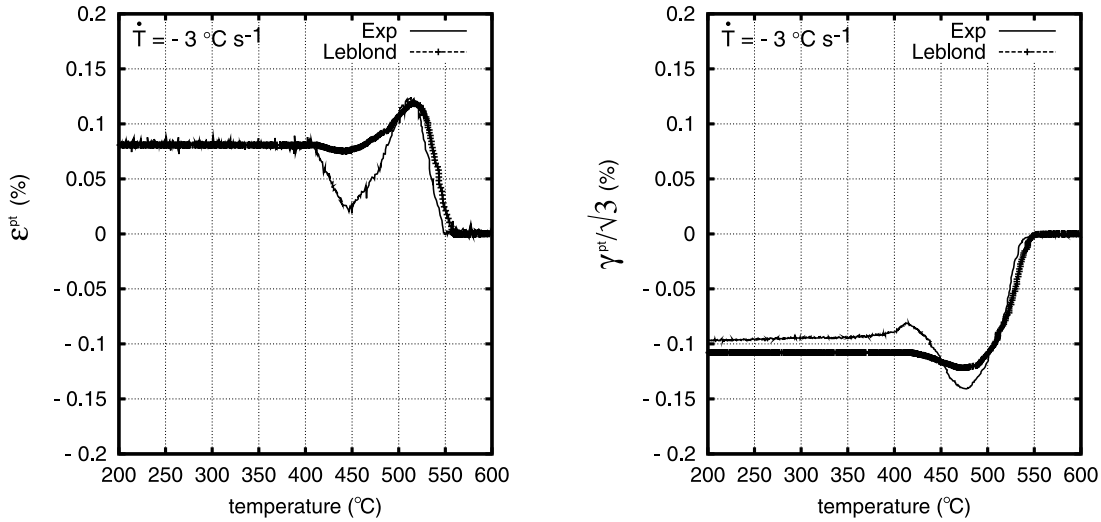

Fig. 27. Transformation-induced plastic strains – comparison with the prediction of Leblond's model.

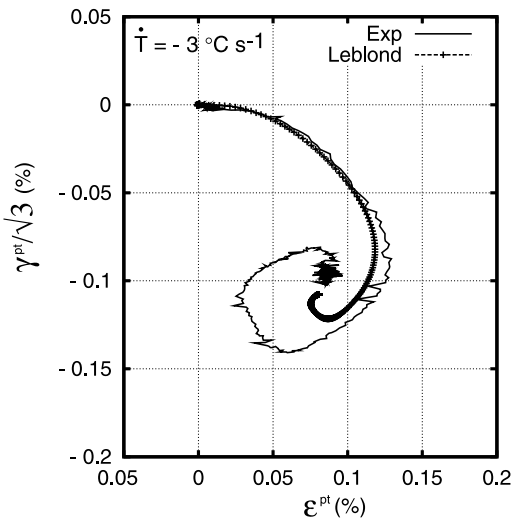

Fig. 28. Evolution of the shear component of the transformation-induced plastic strains vs. the axial component – comparison with the prediction of Leblond's model.

loading cases. Secondly, these tests enabled us to identify Leblond's model through constant stress loading cases and then to compare the response of the model with the experimental data, particularly for the nonproportional load paths. We are able to state that Leblond's transformation plasticity model reproduces the constant stress tests perfectly for the bainitic and austenitic transformations and relatively well in the case of the martensitic transformation for the range of stresses we considered. The simulation of the nonproportional loading tests (on the bainitic transformation) was fairly good in spite of a slight damping effect which prevented the model from matching the experimental results perfectly. A way to improve the model would be the introduction of strain hardening in the transformation-induced plasticity term. We could first implement the isotropic or kinematic hardening model also propose by (Leblond et al., 1989b). Others models suggested by Azzouz et al. (2000), Nagayama et al. (2001) and which take into account the magge effect could bring some more improvements.

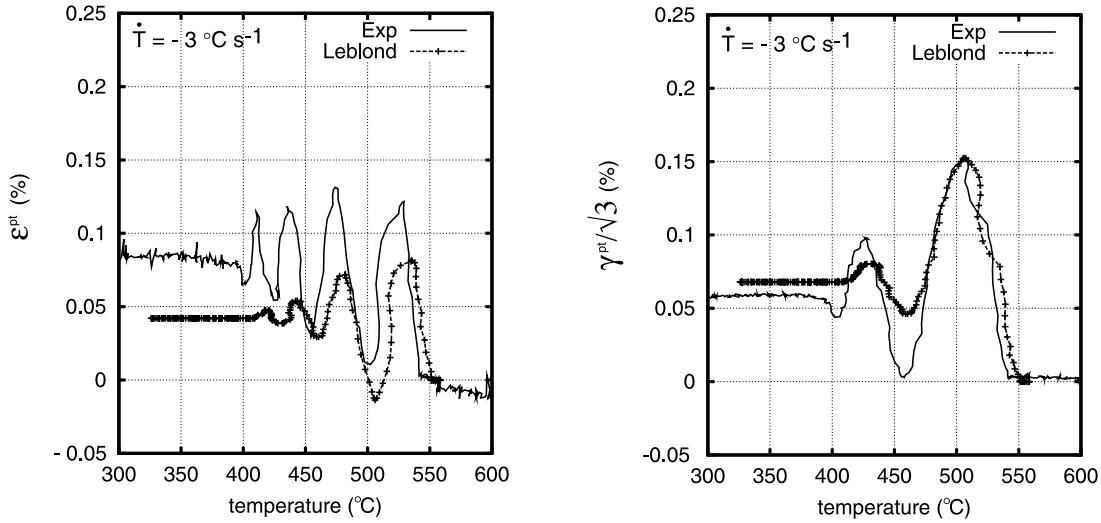

Fig. 29. Transformation-induced plastic strains – comparison with the prediction of Leblond's model.

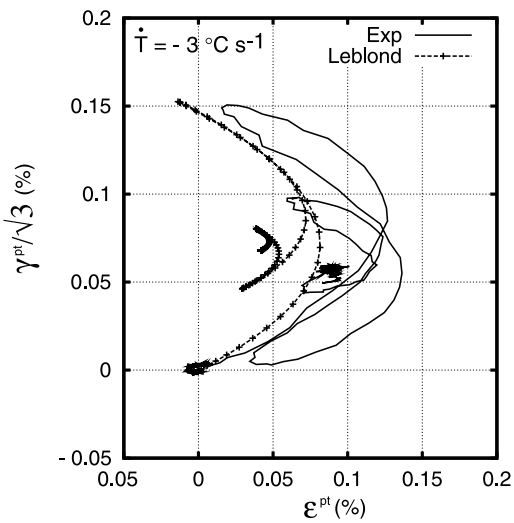

Fig. 30. Evolution of the shear component of the transformation-induced plastic strains vs. the axial component – comparison with the prediction of Leblond's model.

Acknowledgements

Our deepest thanks go to *CEA/DMT*, which sponsored this work, provided the materials and constantly supported our research.

References

Abrassart, F., 1972. Influences des transformations martensitiques sur les propriétés des alliages du système Fe–Ni–Cr–C. Thèse, Université de Nancy.

Azzouz, F., Cailletaud, G., Fischer, F., Nagayama, K., Pineau, A., Tanaka, K., 2000. Back stress development during the austenite–martensite transformation. Z. Angew. Math. Mech. 80.

Cavallo, N., 1998. Contribution à la validation expérimentale de modèles décrivant la ZAT lors d'une opération de soudage. Thèse, INSA Lyon.

Cherkaoui, M., Berveiller, M., 2000. Micromechanical modeling of the martensitic transformation induced plasticity in steels. Smart Mater. Struct. 9, 592–603.

Coret, M., 2001. Étude expérimentale et simulation de la plasticité de transformation et du comportement multiphasé de l'acier de cuve 16MND5 sous chargement multiaxial anisotherme. Thèse, LMT, Cachan.

Coret, M., Calloch, S., Combescure, A., 2002. Experimental study of the phase transformation plasticity of 16MND5 low carbon steel under multiaxial loading. Int. J. Plasticity 18, 1707–1727.

Denis, S., 1996. Considering stress-phase transformation interactions in the caclulation of heat treatment residual stresses. J. Phys. 6, 159–174.

Denis, S., Gautier, E., Simon, A.G.B., 1985. Stress-phase-transformation interaction, basics principle, modelling, and calculation of internal stresses. Mater. Sci. Tech. 1, 805–814.

Denis, S., Gautier, E., Sjöström, S., 1987a. Influence of stresses on the kinetics of pearlitic transfomation during continuous cooling. Acta Metall. 35, 1621–1632.

Denis, S., Sjöström, S., Simon, A., 1987b. Coupled temperature, stress, phase transformation calculation model, numerical illustration of the internal stresses evolution during cooling of a eutectoide carbon steel cylinder. Metall. Trans. 18A, 1203–1212.

Desalos, Y., 1981. Comportement mécanique et dilatométrique de l'auténite métastable de l'acier a533. Rapport No 95 34 94 01, IRSID.

Fernandes, F., Denis, S., Simon, A., 1985. Mathematical model coupling phase transformation and temperature evolution during quenching of steels. Mater. Sci. Techn. 1 (10), 838–844.

Fischer, F., Antretter, T., Azzoua, F., Cailletaud, G., Pineau, A., Tanaka, K., Nagayama, K., 2000a. The role of backstress in phase transforming steel. Arch. Mech. 52, 569–588.

Fischer, F., Reisner, G., Werner, E., Tanaka, K., Cailletaud, G., Antretter, T., 2000b. A new view on transformation induced plasticity (trip). Int. J. Plasticity 16, 723–748.

Giusti, J., 1981. Contraintes et déformations résiduelles d'origine thermique application au soudage et à la trempe des aciers. Thèse, Université P. et M. Curie, Paris IV.

Greenwood, G., Johnson, R., 1965. The deformation of metals under small stresses during phase transformations. Proc. R. Soc. 283, 403–422.

Grostabussiat-Petit, S., 2000. Conséquence mécanique des transformations structurales dans les alliages ferreux. Thèse, INSA Lyon.

Habraken, A., Bourdouxhe, M., 1992. Coupled thermo-mechanical-metallurgical analysis during the cooling process of steel pieces. Eur. J. Mech. A Solids 11 (3), 341–402.

Hamata, N., Billardon, R., Marquis, D., Cheikh, A.B., 1991. A model for nodular graphite cast iron coupling anisothermal elasto-viscoplasticity and phase transformation. In: Desai, C.S., et al. (Eds.), Constitutive Laws for Engineering Materials. ASME Press.

Inoue, T., Wang, Z., 1985. Coupling between stress, temperature, and metallic structures during processes involving phases transformations. Mater. Sci. Tech. 1, 845–850.

Inoue, T., Yamaguchi, Wang, Z., 1985. Stresses and phase transformations occurring in quenching of carburazed steel gear wheel. Mater. Sci. Tech. 1, 872–876.

Leblond, J., Devaux, J., Devaux, J., 1989a. Mathematical modelling of transformation plasticity in steel i. case of ideal-plastic phases. Int. J. Plasticity 5, 551–572.

Leblond, J., Devaux, J., Devaux, J., 1989b. Mathematical modelling of transformation plasticity in steel i. coupling with strain hardening phenomena. Int. J. Plasticity 5, 573–591.

Magee, C., 1966. Transformation kinetics, microplasticity and aging of martensite in FE31Ni, Ph.D. thesis, Carnegie Inst. Technologie, Pittsburg PA.

Martinez, M., 1999. Jonction 16MND5-INCONEL 690-316LN par soudage diffusion elaboration et calcul des contraintes résiduelles de procédé. Thèse, ENSMP.

Mizushima, 1984. Rapport matériau. Technical report, Kawasaki steel corporation.

Nagayama, K., Kitajima, Y., Kigami, S., Tanaka, K., Fischer, F., Cailletaud, G., 2000. Transformation induced plasticity in maraging steel: an experimental study. Key Engrg. Mater. 177–180, 443–448.

Nagayama, K., Terasaki, T., Goto, S., Tanaka, K., Antretter, T., Fischer, F., Cailletaud, G., Azzouz, F., 2002. Back stress evolution and iso-volume fraction lines in a Cr–Ni–Mo–Al–Ti maraging steel in the process of martensitic transformation. Mater. Sci. Engrg. A 336, 30–38.

Nagayama, K., Terasaki, T., Tanaka, K., Fischer, F., Antretter, T., Cailletaud, G., Azzouz, F., 2001. Mechanical properties of a Cr–Ni–Mo–Al–Ti maraging steel in the process of martensitic transformation. Mater. Sci. Engrg. A 308, 25–37.

Sjöström, S., 1985. Interactions and constitutive models for calculating quench stresses in steel. Mater. Sci. Tech. 1, 823–829.

Taleb, L., Cavallo, N., Waekael, F., 2000. Experimental analysis of transformation plasticity. Int. J. Plasticity 0, 1–20.

Taleb, L., Sidoroff, F., 2003. Micromechanical modelling of Greenwood–Johnson mechanism in transformation induced plasticity. Int. J. Plasticity 19, 1821–1842.

Tanaka, K., Terasaki, T., Goto, S., Fischer, F., Antretter, T., Cailletaud, G., 2003. Effect of back stress evolution due to martensitic transformation on iso-volume lines in a Cr–Ni–Mo–Al–Ti maraging steel. Mater. Sci. Engrg. A 341, 189–196.

Todinov, M., 1998. Mechanism for formation of the residual stresses from quenching. Modelling Simul. Mater. Engrg. 6, 273–291.

Videau, J., Cailletaud, G., Pineau, A., 1996. Experimental study of the transformation-induced plasticity in a Cr–Ni–Mo–Al–Ti steel. J. Physique 6, 465–474.

Waeckel, F., 1994. Une loi de comportement thermo-métallurgique des aciers pour le calcul mécanique des structures. Thèse, ENSAM.